AMERICAN SOCIETY FOR MICROBIOLOGY | Microbiology Spectrum

RESEARCH ARTICLE

All Driven by Energy Demand? Integrative Comparison of Metabolism of *Enterococcus faecalis* Wildtype and a Glutamine Synthase Mutant

Seyed Babak Loghmani,[a] Eric Zitzow,[b] Gene Ching Chiek Koh,[c]* Andreas Ulmer,[d] Nadine Veith,[a] Ruth Großeholz,[a] Madlen Rossnagel,[b] Maren Loesch,[d] Ruedi Aebersold,[c] Bernd Kreikemeyer,[b] Tomas Fiedler,[b] Ursula Kummer[a]

[a]Department of Modelling of Biological Processes, BioQuant/COS Heidelberg, Heidelberg University, Heidelberg, Germany
[b]Institute for Medical Microbiology, Virology and Hygiene, Rostock University Medical center, Rostock, Germany
[c]Department of Biology, Institute of Molecular Systems Biology, ETH Zurich, Zurich, Switzerland
[d]Institute of Biochemical Engineering, University of Stuttgart, Stuttgart, Germany

ABSTRACT Lactic acid bacteria (LAB) play a significant role in biotechnology, e.g., food industry and also in human health. Many LAB genera have developed a multidrug resistance in the past few years, causing a serious problem in controlling hospital germs worldwide. *Enterococcus faecalis* accounts for a large part of the human infections caused by LABs. Therefore, studying its adaptive metabolism under various environmental conditions is particularly important to promote the development of new therapeutic approaches. In this study, we investigated the effect of glutamine auxotrophy (Δ*glnA* mutant) on metabolic and proteomic adaptations of *E. faecalis* in response to a changing pH in its environment. Changing pH values are part of the organism's natural environment in the human body and play a role in the food industry. We compared the results with those of the wildtype. Using a genome-scale metabolic model constrained by metabolic and proteomic data, our integrative method allows us to understand the bigger picture of the adaptation strategies of this bacterium. The study showed that energy demand is the decisive factor in adapting to a new environmental pH. The energy demand of the mutant was higher at all conditions. It has been reported that Δ*glnA* mutants of bacteria are energetically less effective. With the aid of our data and model we are able to explain this phenomenon as a consequence of a failure to regulate glutamine uptake and the costs for the import of glutamine and the export of ammonium. Methodologically, it became apparent that taking into account the nonspecificity of amino acid transporters is important for reproducing metabolic changes with genome-scale models because it affects energy balance.

IMPORTANCE The integration of new pH-dependent experimental data on metabolic uptake and release fluxes, as well as of proteome data with a genome-scale computational model of a glutamine synthetase mutant of *E. faecalis* is used and compared with those of the wildtype to understand why glutamine auxotrophy results in a less efficient metabolism and how—in comparison with the wildtype—the glutamine synthetase knockout impacts metabolic adjustments during acidification or simply exposure to lower pH. We show that forced glutamine auxotrophy causes more energy demand and that this is likely due to a disregulated glutamine uptake. Proteome changes during acidification observed for the mutant resemble those of the wildtype with the exception of glycolysis-related genes, as the mutant is already energetically stressed at a higher pH and the respective proteome changes were in effect.

KEYWORDS *Enterococcus faecalis*, glutamine synthetase mutant, pH adaptation

Editor John M. Atack, Griffith University

Address correspondence to Ursula Kummer, Ursula.Kummer@bioquant.uni-heidelberg.de.

*Present address: Gene Ching Chiek Koh, MRC Cancer Unit, University of Cambridge, Cambridge, UK.

The authors declare no conflict of interest.

Received 10 December 2021
Accepted 12 January 2022
Published 2 March 2022

Lactic acid bacteria (LAB) are Gram-positive microorganisms, fermenting hexose sugars to lactic acid as their primary product under many conditions. Among LABs there are both pathogenic as well as commensal species. In some cases, e.g., in the case of *Enterococcus faecalis* both commensal, as well as pathogenic behavior occurs (1). As a part of the commensal flora, *E. faecalis* colonizes different tracts in the human body, especially the gut. Due to its pathogenic potential, *E. faecalis* frequently causes nosocomial infections, most commonly of the urinary tract, but also soft tissue or intra-abdominal infections, bacteremia or endocarditis (2). An increasing proportion of *E. faecalis* strains isolated from such infection shows multidrug resistance against a wide range of antibiotics (3, 4). These multi-resistant *E. faecalis* strains may cause severe problems in hospital environments as treating such infections can be remarkably hard (5).

On the other hand, *E. faecalis* strains generally regarded as safe (GRAS) are used in the food industry as a cheese starter culture (6) or as a probiotic (7). However, the intended probiotic isolates should undergo screening to ensure the absence of transferable virulence factors and antibiotic resistance genes (8). Hence, *E. faecalis* encounters very different native environments ranging from different human body tissues to different kinds of food. This requires enormous flexibility of the metabolism of *E. faecalis* as can be reflected by the various metabolic phenotypes.

To gain a comprehensive understanding of metabolic phenotypes, cell-wide and integrative analysis of metabolism is crucial. This is something that pure experimental research cannot deliver, and therefore, different computational approaches have been developed to study metabolic networks. For smaller networks and more detailed analysis, kinetic models based on ordinary differential equations (ODEs) are the best choice (9). When integrating all reactions of the metabolic network and in the absence of detailed kinetic data, genome-scale metabolic models, as used below, are nowadays the preferred and most commonly used strategy. Genome-scale metabolic models are stoichiometric representations of all annotated metabolic reactions in a given cell which allow the computation of flux distributions based on the knowledge of their localization, wiring, and the biomass composition of the specific organism and/or cell type (10). Optimal flux distributions are calculated according to an optimality criterion like biomass maximization (11). This is an especially successful criterion for investigating microorganisms since these often follow relatively simple principles like optimizing growth. However, the typical outcome of such an optimization (flux balance analysis [FBA]) is not a unique solution and the huge size of the solution space renders interpretation of the results difficult and error-prone (12). By adding constraints, e.g., through experimentally measured medium composition, input and output fluxes of metabolites (13), transcriptome (14), and proteome data (15), the solution space can effectively be decreased and the predictive power of the models increased (15, 16).

In this study, we analyzed the metabolic and proteomic profile of a knockout mutant of the glutamine synthetase (Δ*glnA)* of the multi-resistant *E. faecalis* V583 strain during a pH shift experiment. Glutamine synthetase (GlnA) is a crucial protein as it is the main enzyme in the assimilation of ammonia and has overall control over the nitrogen metabolism (17). We designed an experiment to investigate the effect of glutamine auxotrophy on the metabolic behavior of the organism under two pH conditions by comparing the results to those of the wildtype (18). For this purpose, a previously published genome-scale metabolic model (19) of the wildtype was adjusted to represent the Δ*glnA* mutant. Experimental data of the Δ*glnA* mutant were then used to constrain the solution space of the model. The results were compared with a likewise constrained wildtype model, thereby providing an integrative view on the metabolic adjustments that the organism has to perform to react to the imposed glutamine auxotrophy during environmental pH changes.

RESULTS

In order to follow the metabolic adjustments to pH changes in the Δ*glnA* mutant of *E. faecalis* V583, a chemostat set-up was used, and a pH shift from pH 7.5 to 6.5 was

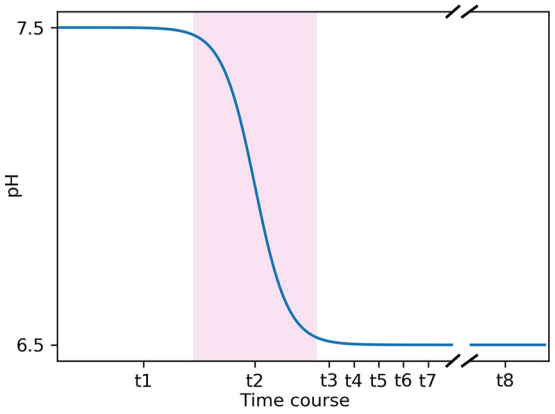

FIG 1 Time course of the pH shift experiment. Samples were taken at t1 (steady-state at pH 7.5), t2 (the transition state [pink background] during the pH shift), t3, t4, t5, t6, and t7, which indicate data points at pH 6.5 at 80, 100, 120, 180, and 240 min after the start of the pH shift. Finally, samples were taken at t8, the steady-state at pH 6.5, 21 h after the start of the experiment. The distance between the data points does not represent the actual time difference in the experiment. Also, the break between t7 and t8 shows the shortened x axis between the two data points.

applied (Fig. 1). Samples were taken and subjected to biomass, metabolite, and proteome measurements at all indicated time points. The results are compared with earlier measurements of the corresponding *E. faecalis* wildtype strain under the same conditions (18).

Effect of pH on the growth rate. The biomass production of *E. faecalis* Δ*glnA* decreased from 1.54 to 1.15 g/L when the pH was shifted from 7.5 to 6.5 (Fig. 2). The trend of decreasing biomass production at lower pH values is similar to the wildtype, as the biomass production in both genotypes decreased by approximately 25%. However, the biomass production of the wildtype at any given pH value is larger than that of the mutant, suggesting an important role of the glutamine synthetase reaction for the growth of the organism.

The effect of pH on metabolite uptake and production. To discover the effect of a pH shift on the metabolic behavior of *E. faecalis* Δ*glnA*, concentrations of the extracellular carbon source (glucose), organic acids, and amino acids were determined in the samples of the chemostat experiment and the respective uptake or production rates were calculated accordingly (Fig. 3). The measured profile of the carbon source and organic acids consists of the uptake rate of glucose as the primary energy source for the organism, and the fermentation profile containing lactate, acetate, ethanol, and formate. Collectively these measurements reflect the state of the energy metabolism at each pH value. Similar to the wildtype, the glucose uptake rate increased in response to the drop in pH, indicating a higher energy demand in a more acidic environment.

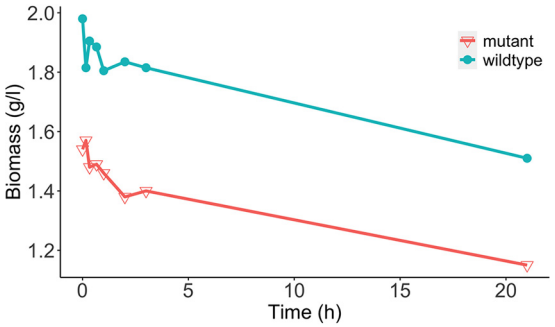

FIG 2 Development of the biomass production over 21 h during the pH shift experiment. The red line shows the biomass values of the *E. faecalis* Δ*glnA* mutant, while the blue line shows the one of the wildtype. Each data point represents the mean of two biological replicates.

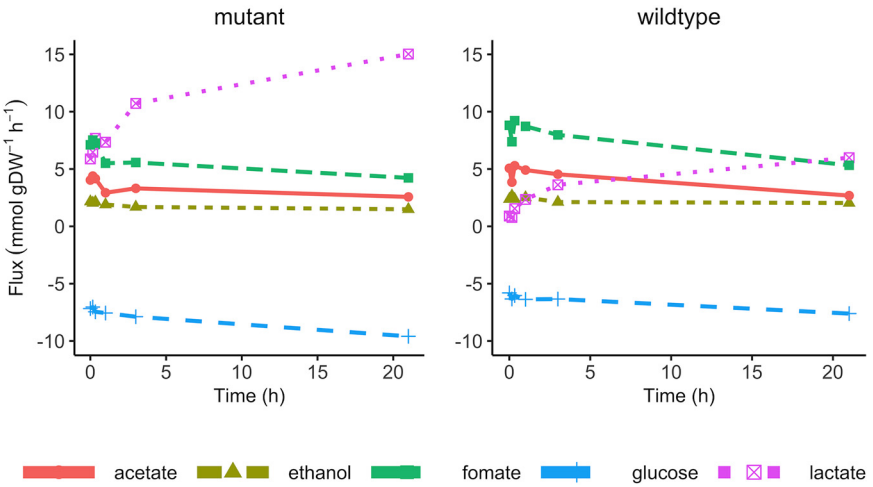

FIG 3 The uptake and production rate of glucose and fermentation products during the pH shift experiment. The left panel shows the data from the mutant, and the right panel shows the data from the wildtype. Each data point represents the mean of two biological replicates.

This is mostly caused by the need to pump protons (leaked into the cell) out of the cell at the expense of ATP (18). Moreover, the fermentation pattern changed from mixed acid fermentation to homolactic fermentation, as homolactic fermentation is often used under more energetically demanding conditions (20). Despite these qualitative similarities of the pH response of the mutant strain to that of the wildtype, quantitatively, the increase in energy demand is much more pronounced in the mutant. This is reflected in a higher lactate production and in the extent of the shift to homolactic fermentation. Therefore, in summary, these results indicate a higher energy demand in the Δ*glnA* mutant of *E. faecalis* compared to the wildtype at all pH values.

This increased energy demand is also evident when comparing amino acid uptake and production rates between *E. faecalis* Δ*glnA* and the wildtype (Fig. 4). Overall, the amino acids uptake rate decreased in response to pH shift except for arginine, glutamine, and serine. Because less biomass is produced and more ATP is needed for proton export, less protein synthesis should occur reflected by decreased amino acid uptake. At the same time, amino acid uptake is also energy-consuming because it is accompanied by either direct ATP consumption or additional proton import. Therefore, it is interesting to look at the reason for an increased uptake rate under these conditions. The uptake rate of arginine and serine, as well as the production rate of ornithine both increased in the wildtype and the mutant after the pH shift. It has been reported that a variety of lactic acid bacteria use the catabolism of arginine via arginine deiminase in response to a more acidic environment (21). Initially, it had been believed that there is a beneficial buffering by ammonia. But, when calculating the actual stoichiometries, we previously showed that this is not the case at the respective pH and reference 13. However, arginine is readily metabolized to gain ATP, which can be used to pump protons to the extracellular environment under a more acidic condition. Therefore, it can be suggested that under more energy-demanding conditions (mutant *versus* wildtype, pH 6.5 *versus* 7.5), a higher uptake rate of arginine may help cells to boost energy production. Serine uptake was also increased after the pH shift in the Δ*glnA* mutant, as serine can also be used for ATP production via degradation to ammonia and pyruvate and fermenting pyruvate to acetate.

Additionally, the increase in glutamine uptake and ammonia production were considerably higher in the mutant compared with the wildtype at both pH levels. Obviously, the mutant would take up more glutamine due to glutamine auxotrophy. The glutamine auxotrophy of the mutant might be the reason for the larger margin between the two pH values compared to the wildtype. This can possibly be explained by a previous report

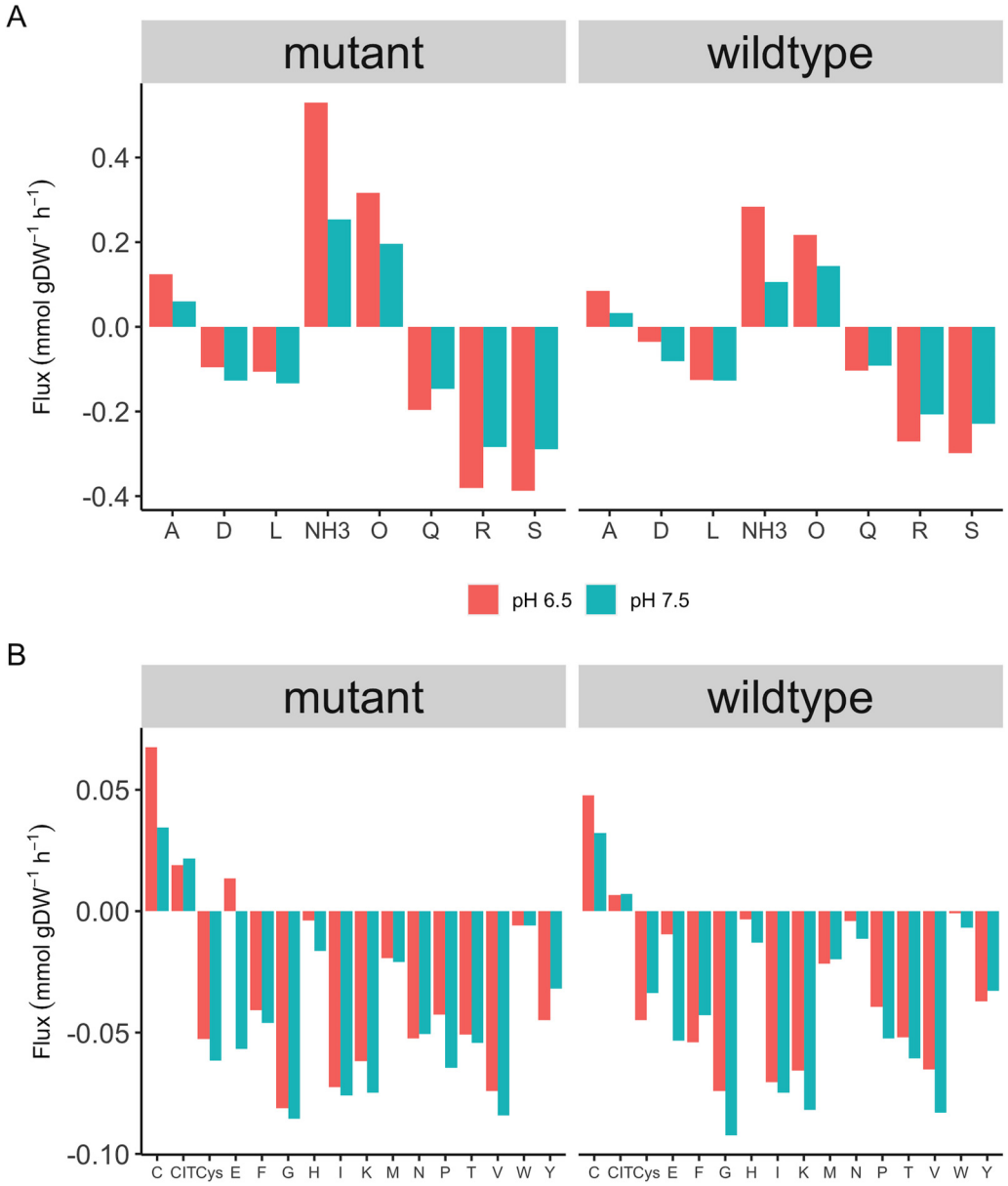

FIG 4 The uptake and production of the amino acids in the wildtype and the Δ*glnA* mutant at pH 7.5 and 6.5 (t1 and t8, respectively). Panel A shows the uptake/production rate of amino acids with high flux value (larger than 0.1 mmol/$g^{-1}_{DW}h^{-1}$), and panel B shows the uptake/production rate of amino acids with low flux value (smaller than 0. mmol/$g^{-1}_{DW}h^{-1}$). Significant fold changes on protein level during the pH shift.

that in *Streptococcus pneumoniae* (22) the transcription factor GlnR (which controls the production and transport of glutamine) depends on the intact gene for GlnA to successfully function. Therefore, a loss of function mutation in GlnA might result in the upregulation of the glutamine ABC transporter (GLNabc) and an unnecessarily high glutamine uptake rate accordingly.

To observe the effect of the pH shift on protein expression in *E. faecalis* Δ*glnA*, the expression rate of all detected proteins was quantified throughout the pH shift experiment, and the respective significant fold changes were calculated at different time points compared with time point 1 (t1) (Fig. 5). The complete set of significantly changed protein expressions is shown in the supplement (Table S10 to 15). While there was no significant fold change at t2, the highest number of fold changes was observed at t3, 20 min after reaching pH 6.5, with more than 40 proteins (out of 1,681 detected

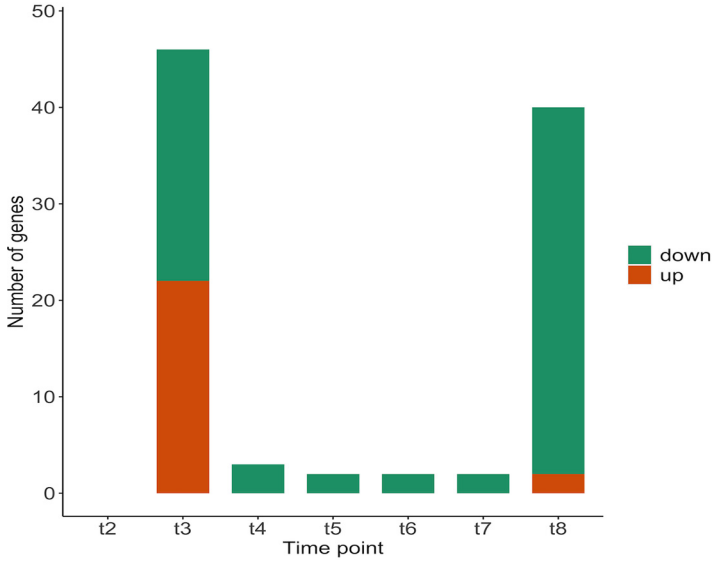

FIG 5 The significant change in protein abundances in the Δ*glnA* mutant during the pH shift experiment at different time points.

ORFs) being affected. Among all affected proteins, 11 are involved in membrane and cell wall production, and two proteins were assigned to reactions involved in peptidoglycan biosynthesis. This suggests that restructuring of the membrane and cell envelope occurs early in response to a change in environmental pH—similar to what has been observed for the wildtype (18). A smaller number of proteins was affected by the pH shift between t4 (40 min after reaching pH 6.5) and t7 (4 h after the start of the pH shift), all of which were downregulated. At t8, 21 h after the pH shift, the number of significant fold changes amounted to 40, with the majority of the proteins being downregulated. A large number of these is involved in nucleotide biosynthesis (Table 1). Considering the fact that *de novo* biosynthesis of nucleotides is an energy-demanding process for the organism, the downregulation of the respective pathways is in line with the higher energy demand under the more acidic condition.

To determine the differences between the wildtype and the mutant at the proteome level, we compared the significant changes in protein abundances for both genotypes during the pH shift experiment (Fig. 6). Except for t8, the number of significant fold changes in the wildtype was considerably higher than that in the mutant.

As previously mentioned, at early time points, both the mutant and the wildtype showed fold changes in enzymes that are involved in membrane and cell wall production. However, after pH shift, the wildtype also displayed an upregulation of glycolytic enzymes at these early time points. The lack of increased expression in glycolytic enzymes in the mutant might be explained by the previously introduced higher energy demand. Because glycolysis is responsible for the major energy production in *E. faecalis*, it is plausible that the expression of those enzymes was already at a higher level in the mutant. The downregulation of enzymes involved in nucleotide metabolism after the pH shift is again similar between wildtype and mutant.

Computational. To study the metabolic behavior of *E. faecalis* Δ*glnA* more compre-

TABLE 1 The number of significant changes in protein abundances and the prominent respective subsystems at t8 (Δ*glnA* mutant)

Subsystems	No. of affected genes
Amino acid metabolism	3
Carbohydrate metabolism	7
Nucleotide metabolism	22
Transport	6

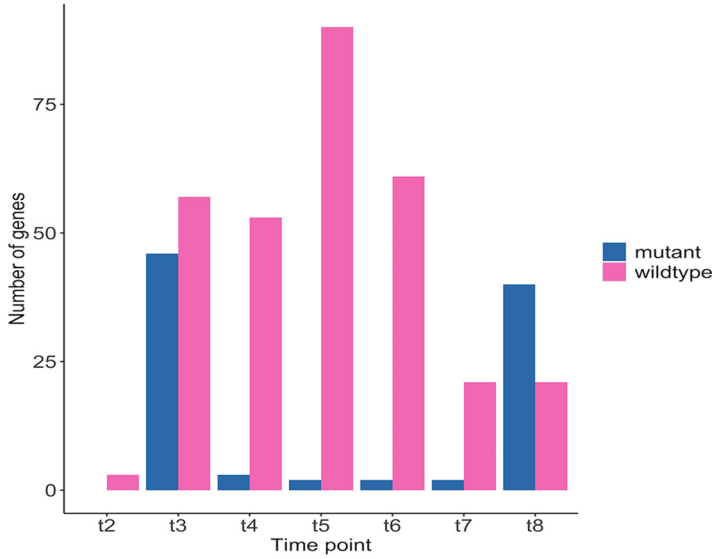

FIG 6 The number of significant changes in protein abundances during the pH shift experiment in the wildtype and the Δ*glnA* mutant.

hensively and on a cell-wide scale, we applied a combination of genome-scale modeling and experimentally determined constraints. For that matter, the previously published genome-scale metabolic network of *E. faecalis* (19) was used to simulate the pH shift experiment by integrating metabolic and proteomic data from the *E. faecalis* Δ*glnA*. To integrate the experimental data into the genome-scale model, the framework from our previous (18) work was applied. To represent the *glnA* knockout in the model, the reaction flux of glutamine synthetase was set to zero. The complete model is available at BioModels (23).

Determination of the non-growth-associated ATP value of *E. faecalis* Δ*glnA*. In order to prepare the genome-scale model of *E. faecalis* Δ*glnA* for the integration of the above-described data and the analysis *via* FBA, we determined the non-growth-associated energy demand (ATPm), which is an important feature for performing FBAs. The non-growth-associated energy demand reflects the amount of energy required to sustain life at zero growth. Thus, the definition of this parameter is an important aspect for genome-scale modeling as it can strongly affect the flux distributions in the metabolic network.

For this purpose, *E. faecalis* Δ*glnA* was grown in chemostat cultures at two different dilution rates (0.05, 0.15 h^{-1}). After reaching the steady-state, samples were taken from the chemostat cultures and the metabolite composition in the supernatant was experimentally determined to calculate the uptake/production rate of extracellular metabolites. The uptake and production rates of glucose, organic acids, and amino acids were then integrated into the model as reaction constraints, defined as bounds on the respective exchange reactions. To calculate parameters for the ATPm reaction for each dilution rate, the biomass production reaction was fixed at the maximal growth rate that is equal to the value of the dilution rate, and the flux through the ATPm reaction was maximized as the new objective function. The obtained maximal objective function value, namely, the maximal flux through the ATPm reaction at different dilution rates, is plotted against the respective dilution rate and a linear function was fitted to those values. The non-growth-associated energy reflects the amount of energy that microbes require to survive at zero growth and is derived from the *y*-intercept of the linear function. This value represents the maintenance energy and was used as the lower bound of the ATPm reaction in the model.

This constraint ensures that the minimum required amount of energy for non-growth-associated purposes is produced by the model and is not channeled into biomass

production and thus into growth. As a result, the calculated value of ATPm of the *E. faecalis* Δ*glnA* was 5.977 and 6.224 mmol/$g^{-1}_{DW}h^{-1}$ at pH 7.5 and 6.5, respectively. When integrated into the model, however, the maximal biomass production is too high compared with experimental data. This is due to the fact that the very high ATP production, which is associated with this value of ATPm, leads to some ATP being redirected toward biomass production. Hence, the constraints of this reaction had to be set on a higher value under both pH conditions. Several reasons allow for such adjustment without violating the modeling rules. First, the ATPm is an estimated value by taking the measured value of around 30 metabolites into account. Therefore, the estimation is very error-prone, as the measurement errors of all the metabolites accumulate and impact the optimization process. For instance, the glucose uptake rate at pH 7.5 at the dilution rate of 0.15 was 6.32 mmol/$g^{-1}_{DW}h^{-1}$ in the data set used for ATPm estimation, and 7.17 mmol/$g^{-1}_{DW}h^{-1}$ in another previously measured data set shown in Fig. 3. This difference of 0.85 mmol/$g^{-1}_{DW}h^{-1}$ results in approximately 2 mmol/$g^{-1}_{DW}h^{-1}$ difference at the optimized ATPm value at this particular condition. Second, the ATPm value, in essence, is meant to ensure that the model is not reaching the optimal growth by overlooking the non-growth-associated energy. In this sense, deviation from the estimated value to a higher value does not violate the underlying assumption, while deviation to a lower value would require more solid evidence. Here, both calculated values for the ATPm reaction seem to be too low and had to be increased. If we consider lactate production as an indicator of the energetic state of the cell, the fact that the lactate production in the mutant is several times higher than in the wildtype suggests a much higher ATPm value for the mutant compared with the wildtype (the ATPm values in the wildtype were calculated to be 3.9 mmol/$g^{-1}_{DW}h^{-1}$ at pH 7.5 and 8.4 mmol/$g^{-1}_{DW}h^{-1}$ at pH 6.5 [18]). Therefore, the ATPm values in the mutant were increased to 9.7 mmol/$g^{-1}_{DW}h^{-1}$ and 10.6 mmol/$g^{-1}_{DW}h^{-1}$ at pH 7.5 and 6.5, respectively. For pH 7.5, this represents the minimal value for the correct reproduction of biomass production. For pH 6.5, we selected a higher value but noted that the exact value does not considerably impact the solution. These values allowed for a precise reproduction of the biomass and the production rates of the organic acids. It is necessary to point out that under both pH conditions, in addition to being glucose-limited, the chemostat cultures were also deprived of glutamine, suggesting that the glutamine content of the CDM-LAB might be limiting and might thus be insufficient to fulfill the demands in *E. faecalis* Δ*glnA*.

Predicted flux through the energy metabolism in the Δ*glnA* mutant. The experimentally measured metabolic and proteomic data were integrated into the Δ*glnA* genome-scale model to simulate the pH shift experiment (as described for the wildtype [18]). Thus, in short, the uptake and release fluxes are set as boundaries for the respective fluxes and fluxes associated with proteins not present in the proteome data are set to zero, if not essential. Finally, adjustments of flux bounds according to de- or increases in expression are implemented.

As reflected by the experimental data, the Δ*glnA* mutant has a higher energy demand before and after the pH shift. This obviously also holds true in the model after the integration of experimental data. The model shows an increased flux through glycolysis after the pH shift, which implies a higher ATP production. Accordingly, the predicted flux through lactate dehydrogenase (LDH) is also increased after the pH shift.

The flux distribution in glycolysis was compared between wildtype and mutant to investigate the difference in flux values in energy metabolism. At pH 7.5 a higher flux passed through the glycolytic reactions in the mutant as a result of the higher energy demand. One might suspect that the higher energy demand in the mutant results from the need to import glutamine from the extracellular environment either *via* the GLNabc (glutamine ATP binding cassette) transporter or via glutamine permease. The GLNabc-mediated uptake of glutamine consumes ATP and permease-mediated uptake imports protons into the cell, which subsequently increases the ATP demand as ATP is required to pump protons out of the cell. However, glutamine synthesis from glutamate would of course also consume one ATP per glutamine. Therefore, the striking difference in energy demand is still not explained. We will come back to this point below.

Impact of glutamine uptake in the model of *E. faecalis* Δ*glnA*. As explained above, the fact that the Δ*glnA* mutant is unable to produce glutamine leads to increased uptake of extracellular glutamine. Based on the chemostat data, the glutamine uptake increased from t1 at pH 7.5 to time point 8 at pH 6.5, corresponding to a 34% increase from 0.147 mmol/$g^{-1}_{DW}h^{-1}$ to 0.197 mmol/$g^{-1}_{DW}h^{-1}$, respectively. Originally, the glutamine transport via the glutamine ABC transporter (R_GLNabc) and glutamine permease (R_Glnt6) were represented in the model. As proteome data suggested, the ATP binding subunit of the GLNabc (EF0760) was upregulated after the pH shift, suggesting an increase of the transporter demand, which is consistent with the higher uptake rate of glutamine. Considering the fact that membrane proteins were often missing from the proteomic data set (due to technical issues), it is likely that the other subunits of the transporter were subjected to upregulation as well, as there is an increase in glutamine uptake after the pH shift. However, the original design of the glutamine transport in the model could not translate the upregulation of GLNabc into a higher flux. The FBA flux distribution revealed a flux value of zero for GLNabc under both pH conditions.

To gain a consistent result between the model and the experimental data, an improved, new permease reaction was introduced to the model. As reported previously, the permease system in *E. faecalis* is not amino acid-specific, but is rather shared between multiple amino acids with various affinities (24). It is suggested that while glutamine has the highest affinity to the transporter, the same transporter takes up asparagine and threonine as well. Hence, to account for the higher affinity of the transporter for glutamine compared to the other amino acids, we designed the new permease reaction in the model to carry two glutamines together with one asparagine and one threonine and four protons (one per amino acid molecule). The amino acid- specific permeases of all three amino acids were then deactivated accordingly. The new transport design resulted in a successful reproduction of the uptake rate of all three amino acids and also in using GLNabc when a higher uptake rate is in demand after the pH shift. The new set up accounts for the actual transport system in a more accurate way, as it mimics the shared permease system and also gets the ABC transporter in use when needed. The fact that during glutamine uptake involuntarily and automatically other amino acids are taken up as well (expending ATP or taking up protons) might be also at least partially the source for the high energy demand of the mutant. In addition, and as mentioned above, the regulatory effect of GlnR in *E. faecalis* Δ*glnA* might be disrupted so that the uptake of glutamine and the other amino acids transported by the same proteins is less strictly regulated.

Predicted flux through glutamine/glutamate metabolism. The flux distribution of the genome-scale model was subsequently used to analyze the effect of the pH shift on glutamine-glutamate metabolism. This pathway is of particular interest as we aimed to uncover the consequences of glutamine auxotrophy in the metabolism of *E. faecalis* in this study. Following an increase in glutamine uptake and in contrast, decrease in glutamate uptake, the model predicted an upregulation in the glutamine to glutamate conversion, which was reflected in switching on the two reactions, aspartyl-tRNA(Asn): L-glutamine amido-ligase (ADP-forming) (ASNTAL) and carbamoyl-phosphate synthase (glutamine-hydrolysing) (CBPS). This also accounts for the small glutamate excretion in the mutant at pH 6.5 because massive amounts of glutamine will drive the glutamine deaminase to produce both glutamate and ammonium. The glutamate excretion was, however, not observed in a previous study (19). Interestingly, the model predicted a flux shutdown at glutamine-fructose-6-phosphate (gam6p) transaminase, which produces glucose amine-6-phosphate by a transaminase reaction between glutamine and fructose-6-phosphate. Instead, gam6p is produced by assimilating ammonia into fructose-6-phosphate. The model also predicted an increased flux toward the reverse direction of glutamate dehydrogenase (GDH), producing glutamate from 2-oxoglutarate. The directionality of GDH plays an important role in balancing the carbon and nitrogen metabolism (25). The NADPH/NADP ratio is directly influenced by less NADPH

being available for e.g., amino acid biosynthesis when the flux is directed toward glutamate production. This also coincides with our observation of a strongly decreased glutamate uptake from the medium and an increased glutamine uptake (which is required for 2-oxoglutarate production). The decreased level of NADPH also prevents reductive synthesis reactions from taking place, as it is reflected in the significant downregulation of proteins involved in e.g., nucleotide metabolism. As another beneficial side effect, the reverse direction of the GDH consumes one proton. This flux change also leads to a series of changes in other amino acid production/degradation processes. For instance, a higher conversion rate of glutamate to alanine and aspartate was predicted, with the former being excreted by the cell after the pH shift, as also seen in the experimental data.

DISCUSSION

E. faecalis is increasingly important in hospital environments due to the increasing fraction of multi-resistant strains. At the same time, *E. faecalis* is still relevant in the food industry. Therefore, characterizing its metabolism is crucial for understanding this highly adaptable and versatile bacterium. Hence, a thorough analysis of the bacterial metabolism integrating metabolic and proteomic data is a key approach to uncover the strategies underlying their adaptive behavior. In this study, we analyzed the effect of a decline in environmental pH from 7.5 to 6.5 on a Δ*glnA* mutant of *E. faecalis* and compared the results with those of the wildtype (18). Like the wildtype, the Δ*glnA* mutant responded to the pH shift by reprogramming its metabolic and proteomic profile to fit the increased energy demand that comes with the need to maintain a higher pH by pumping protons out of the cell. Many findings, therefore, paralleled the results from the wildtype, thereby also confirming these. However, there are also striking differences, mostly concerning the quantity of the energy demand in the genotypes.

Similar to the wildtype, the mutant decreased biomass production during pH shift because less ATP is available for anabolic processes. In addition, there is a pronounced shift from mixed acid to homolactic fermentation. While the qualitative pattern in the mutant resembled the one in the wildtype, the proportion of lactate production in the mutant was considerably higher. This confirms that under more energy-demanding conditions (Δ*glnA* mutant or acidic conditions), *E. faecalis* changes its fermentation profile to homolactic fermentation. While the stoichiometric analysis of the fermentation pathway shows that mixed acid fermentation produces one more ATP, it is widely reported that LAB species such as *L. lactis* and *L. plantarum* choose homolactic fermentation during high glycolytic flux, high substrate availability, or faster growth rates (20). The high uptake rate of glucose under energetically demanding conditions, which further translates into a higher glycolytic flux, increases the NADH/NAD ratio. Reportedly, a higher ratio of NADH/NAD upregulates the activity of lactate dehydrogenase (LDH), e.g., in *L. lactis* (26). While this has been observed in the literature, a plausible explanation on why the less productive (in terms of ATP) fermentation is favored under energetically demanding conditions is still missing.

The amino acid uptake/production profile further underlines the overwhelming influence of the growing energy demand when pH is lowered. The uptake rate of amino acids mostly decreased following the pH shift except for arginine, serine, and glutamine. A decreased amino acid uptake should be a result of regulation when less biomass is produced, and also saves energy, because the uptake is either coupled to even more proton uptake or to ATP hydrolysis. The increased uptake of arginine and serine can be easily explained since these can be directly used for ATP production. Arginine is considered a prolific energy resource in many lactic acid bacteria, especially those important in the food industry (27, 28). An interesting aspect of arginine catabolism in lactic acid bacteria (when used for energy production) is that it often does not result in citrulline production, regardless of using arginine deiminase or not (27, 28). Likewise, our data suggested that an increase in arginine uptake following the pH shift leads to an increase in ornithine, but not citrulline production. The previous finding on

the production of ornithine from citrulline through ornithine carbamoyl transferase in *E. faecalis* (29) was supported by the flux distribution in the genome-scale model. Ornithine is then used by the arginine-ornithine antiporter to import even more arginine into the cell.

Not surprisingly, there is quite a big difference between wildtype and mutant in glutamine/glutamate metabolism and how this is affected by the pH shift. While the uptake rate of glutamate considerably decreased in response to pH shift, the glutamine uptake rate was increased—in the wildtype only very slightly and strongly in the mutant. As discussed above, several mechanisms might contribute to this observation. First, we proposed in accordance with literature on *S. pneumoniae* (22) that the regulatory effect of the transcription factor GlnR on the uptake of glutamine depends on the intact gene for GlnA, and its absence results in an unregulated glutamine uptake. Second, the reversal of the flux of the GDH with its regulatory consequences is only possible if more 2-oxoglutarate is produced, for which glutamine is needed. Third, as learned from the genome-scale model, it is important to consider the lack of specificity of the amino acid uptake mechanisms. Co-transported with e.g., glutamate are amino acids like aspartate that cannot readily be catabolized for energy production. In the case of glutamine, at least small amounts of arginine are also co-transported, which is favorable under high energy demand.

The glutamine synthetase reaction (catalyzed by GlnA) is the main reaction to assimilate ammonium (17). However, here glutamine is imported in such large quantities that some of it has to be deaminated to produce glutamate (so that even a small amount of excretion is observed) and ammonium, which the model also predicted. In the mutant, besides glutamine deamination, the higher uptake of arginine and serine (compared with the wildtype) and their deamination will add to ammonium production with the individual contribution not being clear at this time. Although high concentrations of ammonium are reported to lower the growth rate in bacteria, the underlying reason is suggested to be the general osmotic or ionic effect of ammonium rather than its toxicity (30). The exact mechanism of ammonium export is not known, but likely either ask for proton antiport or ATP, which adds to the energy demand of the mutant.

The analysis of the proteome data again showed a lot of parallel adjustments to pH shift between wildtype and mutant. Here, the decrease of expression in enzymes of the *de novo* biosynthesis of nucleotides which is costly, and also the upregulation of enzymes involved in the restructuring of the cell membrane and cell wall, which is necessary while facing a drop in extracellular pH level in order to decrease proton leak is common between the genotypes. The mutant, however, shows a striking lack of increasing the protein expression of glycolytic enzymes at the beginning of the pH shift experiment. Because there is already a high glycolytic flux in the mutant at the start of the experiment, we assume that the respective changes in core metabolism already happened at this point.

The vast majority of data were reproducible in the genome-scale model. However, the stoichiometry of amino acid uptake reactions had to be adjusted to a realistic depiction of their nonspecificity. To the best of our knowledge, this has not been considered in other genome-scale models of bacteria so far.

Initially, when considering all of the above findings, which mostly reflect the higher need for energy in the mutant, it was not obvious why this higher need arises. Glutamine is the primary nitrogen donor in bacterial cells. High levels of glutamine have to be maintained in order to allow effective transfer of amino-groups (31). This can be accomplished by its synthesis and uptake in the wildtype or its uptake alone in the mutant. At first glance, the energetic cost of glutamine uptake is comparable to its biosynthesis via GlnA. One ATP is needed for GlnA, and the usage of one ATP or proton import is the consequence of glutamine import. However, if the control over glutamine uptake is inhibited due to the lack of GlnA, the potentially uncontrolled and excessive import of glutamine may incur additional cost to the cells. Moreover, both the

automatic co-transport of unwanted amino acids and the need to excrete large amounts of ammonia are certainly costly.

MATERIALS AND METHODS

Experimental. (i) Bacterial strains and culture conditions. *Enterococcus faecalis* V583 Δ*glnA* (19) was grown in batch cultures at 37°C in a chemically defined medium for lactic acid bacteria (CDM-LAB (13), pH 7.5 and 6.5). The CDM-LAB medium contained the following per liter: 1 g K_2HPO_4, 5 g KH_2PO_4, $NaHCO_3$, 0.6 g ammonium citrate, 1 g acetate, 0.25 g tyrosine,0.24 g alanine, 0.5 g arginine, 0.42 g aspartic acid, 0.13 g cysteine, 0.5 g glutamic acid, 0.15 g histidine, 0.21 g isoleucine, 0.475 g leucine, 0.44 g lysine, 0.275 g phenylalanine, 0.675 g proline, 0.34 g serine, 0.225 g threonine, 0.05 g tryptophan, 0.325 g valine, 0.175 g glycine, 0.125 g methionine, 0.1 g asparagine, 0.2 g glutamine, 10 g glucose, 0.5 g L-ascorbic acid, 35 mg adenine sulfate, 27 mg guanine, 22 mg uracil, 50 mg cystine, 50 mg xanthine, 2.5 mg d-biotin, 1 mg vitamin B_{12}, 1 mg riboflavin, 5 mg pyridoxamine-HCl, 10 mg p-aminobenzoicacid, 1 mg pantothenate, 5 mg inosine, 1 mg nicotinic acid, 5 mg orotic acid, 2 mg pyridoxine, 1 mg thiamine, 2.5 mg lipoic acid, 5 mg thymidine, 200 mg $MgCl_2$, 50 mg $CaCl_2$, 16 mg $MnCl_2$, 3 mg $FeCl_3$, 5 mg $FeCl_2$, 5 mg $ZnSO_4$, 2.5 mg $CoSO_4$, 2.5 mg $CuSO_4$, and 2.5 mg $(NH4)_6Mo_7O_{24}$.

(ii) pH shift experiments in chemostat cultures. The pH shift experiments were carried out as previously described (18). In short, *E. faecalis* V583 Δ*glnA* was grown in glucose-limited chemostat cultures in Biostat B Plus benchtop bioreactors (Sartorius) in 750 mL CDM-LAB with a dilution rate of 0.15/h at 37°C and gassing with 0.05 L/min nitrogen and stirring with 250 rpm. The pH was kept at the desired level by titrating with 2 M KOH. Initially, the pH was kept constant at 7.5 until a steady-state was reached. Steady-state was assumed when no glucose was detectable in the culture supernatant anymore, and dry mass and optical density (600 nm) were constant on two consecutive days. For the pH shift, the pH control was switched off until the desired pH (6.5) value was reached. The cultivation was continued until the steady-state was reached again. Samples were taken at steady state pH 7.5 and at several time points during and after the pH shift as indicated in Fig. 1. Per sampling point, samples for determination of dry mass, extracellular metabolites, and proteomic analysis were taken as previously described (18).

(iii) Chemostat cultures for determination of $ATP_{maintenance}$. For determination of $ATP_{maintenance}$ (ATPm), *E. faecalis* V583 Δ*glnA* was grown in glucose-limited chemostats as described above (except for pH shift) at two different dilution rates, 0.15 h^{-1}, and 0.05 h^{-1}, with three biological replicates per dilution rate. At steady-state samples were taken and processed as described above.

(iv) Quantification of extracellular metabolites. For samples from pH shift experiments, quantification of amino acids in media and culture supernatants was done by Frank Gutjahr Chromotgraphie (Balingen, Germany); quantification of lactate, formate, acetate, glucose, acetoin, 2,3-butanediol, ascorbate, citrate, pyruvate, and ethanol were done by Metabolomics Discoveries GmbH (Potsdam, Germany). For quantification of amino acids, glucose, and fermentation products in CDM-LAB and culture supernatants of samples from $ATP_{maintanance}$ experiments, the following two methods were used.

Method 1: An Agilent 1260 Infinity II HPLC system was used. The system was controlled by OpenLAB CDS Workstation software. For amino acids analysis, sample supernatants were filtered through a 0.22 μm syringe filter into an HPLC sample vial. Amino acids were derivatized, separated on a reversed-phase column (Agilent Poroshell 120 EC-C18 4.6 × 100 mm, 2.7 μm), detected with a diode array detector (DAD G7117A), and quantified following manufacturer's guidelines (AdvanceBio Amino Acid Analysis, © Agilent Technologies, Inc. 2018). Standards ranging from 5 μM to 30 mM were used to quantify aspartate, glutamate, asparagine, serine, glutamine, histidine, glycine, threonine, arginine, alanine, tyrosine, valine, methionine, tryptophan, phenylalanine, isoleucine, leucine, lysine, and proline.

For the analysis of organic compounds, samples were prepared as follows: 100 μL 35% perchloric acid was added to 1 mL sample, mixed, and placed on melting ice for 10 min. Subsequently, 55 μL potassium hydroxide solution (7 M) was added, and the sample was centrifuged for 2 min at 20,000 *g*. The supernatant was filtered through a 0.22-μm syringe filter into an HPLC sample vial. Separation of sugars and fermentation products in the sample was performed by using an Agilent Hi-Plex H column (4.6 × 250 mm, 8 μm) with a working temperature of 65°C using 10 mM H_2SO_4 as a mobile phase with a flow rate of 0.4 mL/min. For detection, a refraction index detector (RID) with a working temperature of 35°C and a diode array detector (DAD) with a wavelength of 210 nm/4 nm with a reference wavelength of 360 nm/100 nm were used. Standards ranging from 50 μM to 150 mM were used for the quantification of glucose, ethanol, citrate, lactate, pyruvate, formate, and acetate.

Method 2: Sugars and organic acids in the supernatant were measured with an isocratic Agilent 1200 series HPLC system equipped with a Phenomenex guard carbo-H column (4 by 3.0 mm) and a Rezex ROA organic acid H (8%) column (300 by 7.8 mm, 8 μm; Phenomenex) maintained at 50°C. Analytes were separated and detected using 5 mM H2SO4 with a constant flow rate of 0.4 mL min^{-1}. Prior to analysis, samples were pretreated for precipitation of abundant phosphate by adding 4 M NH3 and 1.2 M MgSO4 solution, followed by incubation with 0.1 M H2SO4. Absolute concentrations were obtained by standard-based external calibration and normalization with L-rhamnose as internal standard.

(v) Determination of protein abundances. All proteomics experiments and relevant downstream data analyses were done as part of a previous study as essentially described and published in Großeholz et al. (18), where the methods were detailed. The following sections briefly describe the proteome sample preparation and quantification of protein abundances using SWATH-MS.

(vi) Proteome sample preparation. Bacterial cell pellets were washed three times with PBS and

kept frozen until experimentation began. These non-viable cell pellets were processed in two technical replicates using BarocyclerrNEP2320 (PressureBioSciences, Inc, South Easton, MA). Briefly, samples were lysed in buffer containing 8 M urea, 0.1 M ammonium bicarbonate, 10% trifluoroethanol, and completeTM protease inhibitor under pressure cycling (PCT) program (198 cycles, 20 s 45 kpsi, 10 s 0 kpsi) at 35°C. Whole cell lysates were then sonicated for 30 s with 1-min intervals on ice three times. Cellular debris was removed by centrifugation and sample protein concentration was determined by BCA assay prior to protein reduction with 10 mM TCEP for 25 min at 35°C, and alkylation with 40 mM iodoacetamide in the dark for 30 min at room temperature. LysC digestion (1/50, wt/wt) was performed in 6 M urea under PCT program: 90 cycles, 25 s 22 kpsi, 10 s 0 kpsi at 35°C; subsequent trypsin digestion (1/30, wt/wt) was performed at further diluted urea (1.6 M) under PCT program: 180 cycles, 25 s 22 kpsi, 10 s 0 kpsi 35°C. Digestion was stopped by acidification with trifluoroacetic acid (TFA) to a final pH of approximately 2 before C18 column desalting using SEP-PAK C18 cartridges (Waters Corp., Milford, MA, USA).

(vii) Data acquisition and quantification of protein abundances using SWATH-MS. We used available, published SWATH MS Spectral and assay library generated by Großeholz et al. (18). For SWATH-MS data acquisition, the same mass spectrometer and LC-MS/MS setup was operated essentially as described before (32), except that 64 windows of variable effective isolation widths were used (with an additional 1 Da overlap on the left side of the window), with a dwell time of 100 ms to cover the mass range from 400 to 1,200 *m/z* in 3.3 s. The collision energy for each window was set using the collision energy of a 2^+ ion centered in the middle of the window with a spread of 15 eV.

The SWATH targeted data analysis was carried out using (OpenMS 1.12) analysis workflow (OpenSwathWorkflow [33], http://www.openswath.org) running on an internal computing cluster and consists of the following steps. First, fragment-ion chromatograms were extracted for each peptide precursor in its appropriate SWATH-MS window based on the target and decoy assays in TraML format, with an extraction width of 0.05 Thomson (OpenSwath ChromatogramExtractor) and a retention time extraction window of ±300 s around the expected retention time. Additionally, ion chromatograms for the iRT retention time standard peptides were extracted to facilitate projection of the assays from the normalized iRT retention time space into the retention time space for each individual run (OpenSwath RTNormalizer). Peak groups from the extracted fragment-ion chromatograms were formed and scored according to their elution profiles, similarity to the target assay in terms of retention time and relative fragment-ion intensity, as well as features from the full MS2 SWATH spectrum extracted at the chromatographic peak apex (OpenSwath Analyzer). Finally, the optimal separation between true and false peak groups was achieved using a linear discriminant model training with 60-fold semi-supervised learning iterations; and the score distribution from the shuffled decoy assays was used to estimate the false discovery rate using pyProphet (0.9.2) (https://pypi.python.org/pypi/pyprophet21) based on the mProphet algorithm (34) and filtered using 1% FDR at the peptide feature level. Further, peak-groups were aligned among all 48 SWATH runs (24 wt and 24 GlnA mutant samples) using the OpenSwath feature aligner to ensure the consistent quantification of peak groups (peptide features) that could otherwise not be confidently identified above the FDR cut-off from a single run alone. Re-quantification option was also enabled to provide an upper bound for the intensity of target analyte where no peak-group passed the confidence filter so that the final data matrix did not contain any missing data point.

Protein quantification was computed using R package, MSStats.daily 2.3.5 (35). Briefly, we preprocessed the data set from openSWATH extraction by $\log_2$ transformation and quantile normalization and generated the protein quantity matrix from the fragment ion level data using the "groupComparison" and "quantification" function of MSstats.

The mass spectrometry proteomics data have been deposited to the ProteomeXchange Consortium (http://proteomecentral.proteomexchange.org/) via the PRIDE partner repository with the data set identifier PXD030778. Users can sign in via http://www.ebi.ac.uk/pride/archive/ to access the SWATH data with:

Reviewer account details
Username: reviewer_pxd030778@ebi.ac.uk
Password: SfhNDiaz

Computational. (i) Determination of non-growth-associated $ATP_{maintenance}$. The determination of non-growth-associated ATP (ATPm) was performed as described in Teusink et al. (36). Thus, the measured flux value for the carbohydrates, organic acids, and amino acids were integrated in the genome-scale model as constraints (Table S16). The biomass reaction was fixed at the respective growth rate (dilution rate), and the flux of the ATPm reaction was maximized as the objective function. The obtained values were used to fit a linear function, for which the *y*-intercept determines the required energy for the organism at a zero growth rate (Table S17, fig. S1). This value is then applied to the model as the lower bound of the ATPm reaction.

(ii) Software, model, and computational methods. PySCeS-CBMPy (37) was used for constrained-based modeling. The genome-scale metabolic model of *E. faecalis* (19) was used for all the computational analyses (BioModels: MODEL1510010000). To optimize the growth rate, ATPm, and obtaining flux distribution profiles, flux balance analysis (FBA) (11) was used. This method calculates a vector of flux values while optimizing the user-defined objective function. To calculate the feasible range of each reaction that results in the optimized value of the objective function, flux variability analysis (FVA) (38) was applied. FVA uses the optimized value of the objective function as an additional constraint and subsequently calculates the maximum and minimum boundary of the feasible interval for each reaction.

(iii) Integration of constraints to the genome-scale model. The integration of constraints to the genome-scale model was done as indicated in Großeholz et al. (18). To integrate the metabolic data, a

tolerance level of 40% was applied to the measured flux rates to account for measurement errors. The obtained values were applied to the upper (+ 20%) and lower (20%) bounds of the respective exchange reactions at both conditions (Table S2 & S3). Regarding the proteome data, reactions with no experimental evidence (after the comparison to the list of essential genes and reactions (Table S7, S8, & S9) at the proteome level at pH 7.5 were deactivated (Table S4). For the model to have a feasible solution, several genes had to be reactivated (Table S5). To represent the significant fold changes of proteins in response to pH shift, the $\log_2$ fold changes of protein abundances were multiplied by 40% (tolerance level) and then applied to the maximum and minimum value of respective reactions, obtained by flux variability analysis (FVA) (38) at pH 7.5 (Table S6).

Data availability. The raw data of the proteomics experiments for the DglnA mutant of E. faecalis can be found on the PRIDE (Proteomics Identification Database) under the identifier number: PXD030778.

SUPPLEMENTAL MATERIAL

Supplemental material is available online only.

SUPPLEMENTAL FILE 1, PDF file, 0.3 MB.

ACKNOWLEDGMENTS

S.B.L. would like to thank the HGS Mathcomp and the Graduate academy at Heidelberg University for financial support. N.V. and T.F. thank the DFG (grant numbers VE1075/2-1 and FI 1588/2-1) for funding. A.U. and M.L. were funded by the Bundesministerium fuer Bildung und Forschung (BMBF, Funding Number 031B0596B). Ben C. Collins and Olga T. Schubert, the co-authors of Großeholz et al. are acknowledged for proteomics analysis. Ludovic Gillet is acknowledged for submitting the proteomics data to PRIDE.

For the publication fee we acknowledge financial support by the DFG within the funding programme "Open Access Publikationskosten" as well as by Heidelberg University.

REFERENCES

1. Holt JF, Kiedrowski MR, Frank KL, Du J, Guan C, Broderick NA, Dunny GM, Handelsman J. 2015. Enterococcus faecalis 6-Phosphogluconolactonase is required for both commensal and pathogenic interactions with Manduca sexta. Infect Immun 83:396–404. https://doi.org/10.1128/IAI.02442-14.
2. Hancock LE, Murray BE, Sillanpää J. 2014. Enterococcal cell wall components and structures. *In* Gilmore MS, Clewell DB, Ike Y, et al. (eds.), Enterococci: from commensals to leading causes of drug resistant infection. Massachusetts eye and ear infirmary, Boston, MA.
3. Jabbari Shiadeh SM, Pormohammad A, Hashemi A, Lak P. 2019. Global prevalence of antibiotic resistance in blood-isolated Enterococcus faecalis and Enterococcus faecium: a systematic review and meta-analysis. Infect Drug Resist 12:2713–2725. https://doi.org/10.2147/IDR.S206084.
4. Asadollahi P, Razavi S, Asadollahi K, Pourshafie MR, Talebi M. 2018. Rise of antibiotic resistance in clinical enterococcal isolates during 2001–2016 in Iran: a review. New Microbes New Infect 26:92–99. https://doi.org/10.1016/j.nmni.2018.08.018.
5. Kau AL, Martin SM, Lyon W, Hayes E, Caparon MC, Hultgren SJ. 2005. Enterococcus faecalis tropism for the kidneys in the urinary tract of C57BL/6J Mice. Infect Immun 73:2461–2468. https://doi.org/10.1128/IAI.73.4.2461-2468.2005.
6. Dahlberg AC, Kosikowsky FV. 1948. The development of flavor in American cheddar cheese made from pasteurized milk with *Streptococcus Faecalis* Starter. J Dairy Sci 31:275–284. https://doi.org/10.3168/jds.S0022-0302(48)92205-X.
7. Fuller R. 1989. Probiotics in man and animals. J Appl Bacteriol 66:365–378.
8. Baccouri O, Boukerb AM, Farhat LB, Zébré A, Zimmermann K, Domann E, Cambronel M, Barreau M, Maillot O, Rincé I, Muller C, Marzouki MN, Feuilloley M, Abidi F, Connil N. 2019. Probiotic potential and safety evaluation of Enterococcus faecalis OB14 and OB15, isolated from traditional Tunisian Testouri cheese and Rigouta, using physiological and genomic analysis. Front Microbiol 10:881. https://doi.org/10.3389/fmicb.2019.00881.
9. Penkler G, Du Toit F, Adams W, Rautenbach M, Palm DC, van Niekerk DD, Snoep JL. 2015. Construction and validation of a detailed kinetic model of glycolysis in Plasmodium falciparum. FEBS J 282:1481–1511. https://doi.org/10.1111/febs.13237.
10. Oberhardt MA, Palsson BØ, Papin JA. 2009. Applications of genome-scale metabolic reconstructions. Mol Syst Biol 5:320. https://doi.org/10.1038/msb.2009.77.
11. Orth JD, Thiele I, Palsson BØ. 2010. What is flux balance analysis?? Nat Biotechnol 28:245–248. https://doi.org/10.1038/nbt.1614.
12. Bernstein DB, Sulheim S, Almaas E, Segrè D. 2021. Addressing uncertainty in genome-scale metabolic model reconstruction and analysis. Genome Biol 22:64. https://doi.org/10.1186/s13059-021-02289-z.
13. Levering J, Fiedler T, Sieg A, van Grinsven KWA, Hering S, Veith N, Olivier BG, Klett L, Hugenholtz J, Teusink B, Kreikemeyer B, Kummer U. 2016. Genome-scale reconstruction of the Streptococcus pyogenes M49 metabolic network reveals growth requirements and indicates potential drug targets. J Biotechnol 232:25–37. https://doi.org/10.1016/j.jbiotec.2016.01.035.
14. Granata I, Troiano E, Sangiovanni M, Guarracino MR. 2019. Integration of transcriptomic data in a genome-scale metabolic model to investigate the link between obesity and breast cancer. BMC Bioinformatics 20:162. https://doi.org/10.1186/s12859-019-2685-9.
15. Tian M, Reed JL. 2018. Integrating proteomic or transcriptomic data into metabolic models using linear bound flux balance analysis. Bioinformatics 34:3882–3888. https://doi.org/10.1093/bioinformatics/bty445.
16. Reed JL. 2012. Shrinking the metabolic solution space using experimental datasets. PLoS Comput Biol 8:e1002662. https://doi.org/10.1371/journal.pcbi.1002662.
17. Forchhammer K. 2007. Glutamine signalling in bacteria. Front Biosci 12:358–370. https://doi.org/10.2741/2069.
18. Großeholz R, Koh C-C, Veith N, Fiedler T, Strauss M, Olivier B, Collins BC, Schubert OT, Bergmann F, Kreikemeyer B, Aebersold R, Kummer U. 2016. Integrating highly quantitative proteomics and genome-scale metabolic modeling to study pH adaptation in the human pathogen Enterococcus faecalis. NPJ Syst Biol Appl 2:16017. https://doi.org/10.1038/npjsba.2016.17.
19. Veith N, Solheim M, van Grinsven KWA, Olivier BG, Levering J, Grosseholz R, Hugenholtz J, Holo H, Nes I, Teusink B, Kummer U. 2015. Using a genome-scale metabolic model of Enterococcus faecalis V583 to assess amino acid uptake and its impact on central metabolism. Appl Environ Microbiol 81:1622–1633. https://doi.org/10.1128/AEM.03279-14.
20. Teusink B, Bachmann H, Molenaar D. 2011. Systems biology of lactic acid bacteria: a critical review. Microb Cell Fact 10:S11. https://doi.org/10.1186/1475-2859-10-S1-S11.
21. Casiano-Colon A, Marquis RE. 1988. Role of the arginine deiminase system in protecting oral bacteria and an enzymatic basis for acid tolerance. Appl Environ Microbiol 54:1318–1324. https://doi.org/10.1128/aem.54.6.1318-1324.1988.
22. Kloosterman TG, Hendriksen WT, Bijlsma JJE, Bootsma HJ, van Hijum SAFT, Kok J, Hermans PWM, Kuipers OP. 2006. Regulation of glutamine and

glutamate metabolism by GlnR and GlnA in Streptococcus pneumoniae. J Biol Chem 281:25097–25109. https://doi.org/10.1074/jbc.M601661200.
23. Malik-Sheriff RS, Glont M, Nguyen TVN, Tiwari K, Roberts MG, Xavier A, Vu MT, Men J, Maire M, Kananathan S, Fairbanks EL, Meyer JP, Arankalle C, Varusai TM, Knight-Schrijver V, Li L, Dueñas-Roca C, Dass G, Keating SM, Park YM, Buso N, Rodriguez N, Hucka M, Hermjakob H. 2020. BioModels—15 years of sharing computational models in life science. Nucleic Acids Res 48:D407–D415.
24. Holden JT, Bunch JM. 1973. Asparagine transport in Lactobacillus plantarum and Streptococcus faecalis. Biochim Biophys Acta - Biomembr 307:640–655. https://doi.org/10.1016/0005-2736(73)90308-8.
25. Smith EL, Austen BM, B K, N J. 1975. Glutamate dehydrogenases. Enzym 11:29.
26. Garrigues C, Loubiere P, Lindley ND, Cocaign-Bousquet M. 1997. Control of the shift from homolactic acid to mixed-acid fermentation in Lactococcus lactis: predominant role of the NADH/NAD+ ratio. J Bacteriol 179:5282–5287. https://doi.org/10.1128/jb.179.17.5282-5287.1997.
27. Hwang H, Lee J-H. 2018. Characterization of arginine catabolism by lactic acid bacteria isolated from kimchi. Molecules 23:3049. https://doi.org/10.3390/molecules23113049.
28. Tonon T, Lonvaud-Funel A. 2000. Metabolism of arginine and its positive effect on growth and revival of Oenococcus oeni. J Appl Microbiol 89:526–531. https://doi.org/10.1046/j.1365-2672.2000.01142.x.
29. Knivett VA. 1954. The anaerobic interconversion of ornithine and citrulline by Streptococcus faecalis. Biochem J 58:480–486. https://doi.org/10.1042/bj0580480.
30. Müller T, Walter B, Wirtz A, Burkovski A. 2006. Ammonium toxicity in bacteria. Curr Microbiol 52:400–406. https://doi.org/10.1007/s00284-005-0370-x.
31. Reitzer L. 2014. Amino acid synthesis. Elsevier. https://doi.org/10.1016/B978-0-12-801238-3.02427-2.
32. Gillet LC, Navarro P, Tate S, Röst H, Selevsek N, Reiter L, Bonner R, Aebersold R. 2012. Targeted data extraction of the MS/MS spectra generated by data-independent acquisition: a new concept for consistent and accurate proteome analysis. Mol Cell Proteomics 11:O111.016717. https://doi.org/10.1074/mcp.O111.016717.
33. Röst HL, Rosenberger G, Navarro P, Gillet L, Miladinović SM, Schubert OT, Wolski W, Collins BC, Malmström J, Malmström L, Aebersold R. 2014. OpenSWATH enables automated, targeted analysis of data-independent acquisition MS data. Nat Biotechnol 32:219–223. https://doi.org/10.1038/nbt.2841.
34. Reiter L, Rinner O, Picotti P, Hüttenhain R, Beck M, Brusniak M-Y, Hengartner MO, Aebersold R. 2011. mProphet: automated data processing and statistical validation for large-scale SRM experiments. Nat Methods 8:430–435. https://doi.org/10.1038/nmeth.1584.
35. Choi M, Chang C-Y, Clough T, Broudy D, Killeen T, MacLean B, Vitek O. 2014. MSstats: an R package for statistical analysis of quantitative mass spectrometry-based proteomic experiments. Bioinformatics 30:2524–2522. https://doi.org/10.1093/bioinformatics/btu305.
36. Teusink B, Wiersma A, Molenaar D, Francke C, de Vos WM, Siezen RJ, Smid EJ. 2006. Analysis of growth of Lactobacillus plantarum WCFS1 on a complex medium using a genome-scale metabolic model. J Biol Chem 281:40041–40048. https://doi.org/10.1074/jbc.M606263200.
37. Olivier BG, Rohwer JM, Hofmeyr J-HS. 2005. Modelling cellular systems with PySCeS. Bioinformatics 21:560–561. https://doi.org/10.1093/bioinformatics/bti046.
38. Mahadevan R, Schilling CH. 2003. The effects of alternate optimal solutions in constraint-based genome-scale metabolic models. Metab Eng 5:264–276. https://doi.org/10.1016/j.ymben.2003.09.002.